Natural Convective Heat Transfer of Cobalt-kerosene Nanofluid inside a Quarter-Circular Enclosure with Uniform and Non-uniform Heated Bottom Wall Using Two-component Nonhomogeneous Model

Md. Shariful Alam*

Department of Mathematics, Jagannath University, Dhaka-1100, Bangladesh

ABSTRACT

In this paper, the problem of natural convective heat transfer of kerosene-cobalt nanofluid inside a quarter circular enclosure in the presence of oriented magnetic field has been studied numerically using two-component non-homogeneous model. The round wall of the enclosure is maintained at constant low temperature; the left vertical wall is adiabatic whereas the bottom wall is considered as heated uniformly and non-uniformly. The effects of Brownian motion and thermophoresis are incorporated into the nanofluid model. The Galerkin weighted residual finite element method has been employed to solve the governing partial differential equations after converting them into a non-dimensional form using a suitable transformation of variables. Comparison with previously published work is performed and excellent agreement is obtained. The effects of various model parameters such as Hartmann number, Rayleigh number and magnetic field inclination angle on the streamlines, isotherms and isoconcentrations have been displayed graphically for both uniformly as well as non-uniformly heated bottom wall. In addition, the heat transfer augmentation for various model parameters as well as various thermal boundary conditions have been done in light of the average Nusselt number from the bottom heated wall. The obtained numerical results show that the average Nusselt number is an increasing function of the Rayleigh number, while it is a decreasing function of the Hartmann number.

Keywords: Nanofluid; Thermophoresis; Brownian motion; Heat transfer; Finite element method

Introduction

The problem of natural convection in enclosures has many engineering applications such as the cooling systems of electronic components, the building and thermal insulation systems, the built-in-storage solar collectors, the nuclear reactor systems, the food storage industry and the geophysical fluid mechanics. Various techniques have been proposed to enhance

---

*Corresponding author: msalam631@yahoo.com

the convection heat transfer performance of fluids inside the enclosure. Convective heat transfer can be enhanced by changing flow geometry, boundary conditions, and by enhancing thermal conductivity of the fluid.

The influence of a magnetic field on convective flow and heat transfer inside an enclosure has received considerable attention because of a wide variety of application in engineering areas, such as chemical industry, power and cooling industry for drying, chemical vapor deposition on surfaces, cooling of nuclear reactors, crystal growth in liquids, electronic packages, petroleum industries, and microelectronic devices.

Subbarayalu and Velappan [1] studied numerically the magnetoconvection in a tilted square cavity with differentially thermally active vertical walls. The two vertical sidewalls of enclosure are hot and cold surfaces while the horizontal top and bottom walls are adiabatic. Their results confirmed that the average Nusselt number increases with increase in Grashof number but decreases with increase in Hartmann number and behaves in a non-linear fashion with angles of inclination. The effects of the magnetic field on free convection were solved for different cavity shapes such as trapezoidal, rectangular and square. Pirmohammadi and Ghassemi [2] investigated the effect of a magnetic field on laminar natural-convection flow in a tilted enclosure heated from below, cooled from the top and filled with liquid gallium. They found that at Ra=10^4, the value of Nusselt number depends strongly upon the inclination angle for relatively small values of Hartmann number. Lo [3] simulated the effect of a transverse magnetic field on buoyancy-driven magnetohydrodynamic flow in a rectangular enclosure. He showed at a constant value of Gr, the heat transfer rate is maximum for higher Prandtl number and in the absence of magnetic field effects. Bakhshan and Ashoori [4] analyzed a 2-D computational of steady state free convection in a rectangular enclosure filled with an

electrically conducting fluid under the effect of a magnetic field. They observed that Nusselt number and heat flux will increase when increasing Grashof and Prandtl numbers and decreasing the slope of the orientation of magnetic field.

Thus, from the above literatures, it is observed that the effect of the magnetic field on the natural convection inside the enclosure decreases the convection effect and then reduces the heat transfer. Therefore, the addition of nanoparticles to the fluid can improve and increase its thermal performance (since the thermal conductivity of solids is typically higher than that of liquids) and enhance the heat transfer mechanism in the enclosure (see Kakaç and Pramuanjaroenkij [5], Sarit et al. [6], Uddin et al. [7]).

Nanofluids, a name conceived by Choi [8] at Argonne National laboratory, are fluids consisting of solid nanoparticles with size less than 100 nm suspended with solid volume fraction typically less than 4%. Nanofluids can be used to improve thermal management systems in many engineering applications such as transportation, micromechanics and instrument, HVAC system and cooling devices. Recently, many investigators have studied nanofluid convective heat transfer in different geometries both numerically and experimentally. For numerical simulation, two approaches have been adopted in the literature to investigate the heat transfer characteristics of nanofluids, the one-component model and the two-component model. In the one-component model, a uniform volume fraction distribution is assumed for nanofluids. In other words, the viscosity and thermal conductivity of nanofluids are formulated by volume fraction and nanoparticle size, and then continuity, momentum and energy equations are solved for nanofluids. In the two-component model, the volume fraction distribution equation is added to other conservation equations. Buongiorno [9] suggested a two-component

model based on the mechanics of nanoparticles/base-fluid relative velocity. He took the absolute velocity of nanoparticles to be the sum total of the base-fluid velocity and a relative velocity, (which he calls a slip velocity). Considering seven slip mechanisms, namely inertia, Brownian diffusion, thermophoresis, diffusophoresis, Magnus effects, fluid drainage and gravity settling, he concluded that in the absence of turbulent effects, Brownian diffusion and thermophoresis are dominant. Based on these two effects, he derived the conservation equations for nanofluids. Recently, Sheremet and Pop [10] studied free convection in a triangular cavity filled with a porous medium saturated by a nanofluid using the mathematical model proposed by Buongiorno. Their results revealed that the average Nusselt number is an increasing function of the Rayleigh and Lewis numbers and decreasing function of the Brownian motion, buoyancy-ratio and thermophoresis parameters. Very recently, Rahman *et al.* [11] studied Buongiorno's mathematical model for hydromagnetic free convection flow in an isosceles triangular cavity filled with alumina-water nanofluid having different thermal boundary conditions on the bottom wall. Their obtained numerical results indicate that the variable thermal boundary conditions have significant effects on the flow and thermal fields. As per authors' knowledge, the literature review revealed that uniform and non-uniform thermal boundary conditions taking into the Buongiorno's mathematical model in a quarter circular-shapes enclosure which is filled with kerosene-cobalt nanofluid in the presence of oriented magnetic field has not been studied yet. Therefore, in this paper, a finite element simulation has been performed for a quarter circular-shaped enclosure which is filled with kerosene-cobalt nanofluid with uniformly and non-uniformly heated bottom wall in the presence of an oriented magnetic field using Buongiorno's mathematical model.

Mathematical Modeling

A two-dimensional steady laminar natural convective heat transfer and fluid flow inside a quarter circular enclosure filled with kerosene-cobalt nanofluid has been considered. The domain and boundary conditions for the buoyancy-driven heat transfer in the quarter circular enclosure are shown in Fig. 1, where x and y are the Cartesian coordinates, L is the bottom wall length and height of the quarter circular enclosure. A well-defined coordinate system has been fixed, and the gravity worked along the negative y axis. It is assumed that the bottom wall is considered as $T = T_h$ or $T = T_c + (T_h - T_c)(x/L)(1 - (x/L))$. The temperature of the round wall is kept at T_c so that $T_h > T_c$ while the left vertical wall is kept insulated. Due to the uniformly distributed nanoparticles inside the base fluid, the nanoparticle volume fraction on the entire domain has been taken uniform. Thermophoresis and Brownian motion effects are included in this study in the absence of chemical reaction. The base fluid (kerosene) and the solid nanoparticles (cobalt) are in thermal equilibrium. The enclosure is permeated by a uniform magnetic field $\mathbf{B} = B_x e_x + B_y e_y$ of constant magnitude $B_0 = \sqrt{B_x^2 + B_y^2}$, where e_x, e_y are the unit vectors along the coordinate axis. The direction of the magnetic field makes an angle γ with the positive x-axis. The magnetic Reynolds number of the flow is taken to be small enough so that induced magnetic field is assumed to be negligible in comparison with applied magnetic field.
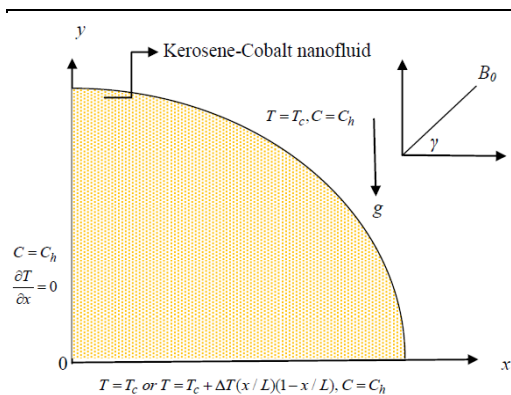
Fig. 1. Physical model of the problem.

The Boussinesq approximation has been applied to consider the density variation. Within the framework of the above-noted assumptions, the governing equations for this model can be written as:

Continuity equation: $\dfrac{\partial u}{\partial x}+\dfrac{\partial v}{\partial y}=0$ (1)

Momentum equation in x -direction:

$$\rho_f[u\frac{\partial u}{\partial x}+v\frac{\partial u}{\partial y}]=-\frac{\partial p}{\partial x}+\mu_f\nabla^2 u$$

$$+\sigma_f B_0^2\left(v\sin\gamma\cos\gamma-u\sin^2\gamma\right) \quad (2)$$

Momentum equation in y -direction:

$$\rho_f[u\frac{\partial v}{\partial x}+v\frac{\partial v}{\partial y}]=-\frac{\partial p}{\partial y}+\mu_f\nabla^2 v$$

$$+\sigma_f B_0^2\left(u\sin\gamma\cos\gamma-v\cos^2\gamma\right) \quad (3)$$

$$+(1-C_0)(T-T_c)\rho_f\beta_f g-(C-C_0)\left(\rho_p-\rho_f\right)g$$

Energy equation:

$$u\frac{\partial T}{\partial x}+v\frac{\partial T}{\partial y}=\alpha_f\nabla^2 T$$

$$+\frac{(\rho c_p)_p}{(\rho c_p)_f}\left\{D_B\left(\frac{\partial C}{\partial x}\frac{\partial T}{\partial x}+\frac{\partial C}{\partial y}\frac{\partial T}{\partial y}\right)\right.$$

$$\left.+\frac{D_T}{T_c}\left[\left(\frac{\partial T}{\partial x}\right)^2+\left(\frac{\partial T}{\partial y}\right)^2\right]\right\} \quad (4)$$

Conservation equation of nanoparticles:

$$u\frac{\partial C}{\partial x}+v\frac{\partial C}{\partial y}=D_B\nabla^2 C+\frac{D_T}{T_c}\nabla^2 T \quad (5)$$

where $\nabla^2=\dfrac{\partial^2}{\partial x^2}+\dfrac{\partial^2}{\partial y^2}$ is the Laplacian operator and other quantities are defined in the nomenclature. In equations (4)-(5), D_B is the Brownian diffusion coefficient and D_T is the thermophoretic diffusion coefficient. The detailed calculations of these two coefficients are given in the works of Uddin et al. [7].

Boundary Conditions

The appropriate boundary conditions for the above stated model are as follows:

(i) On the round wall:

$$u=v=0,\ T=T_c,\ C=C_h \quad (6)$$

(ii) On the bottom wall:

Case-I: $u=v=0$, $T=T_h$, $C=C_h$ (7a)

Case-II: $u=v=0$

$$T=T_c+\Delta T\left(x/L\right)\left(1-\left(x/L\right)\right),\ C=C_h \quad (7b)$$

(iii) On the left vertical wall:

$$u=v=0,\ \frac{\partial T}{\partial x}=0,\ C=C_h \quad (8)$$

Dimensional Analysis

Dimensional analysis is one of the most important mathematical tools in the study of fluid mechanics. To describe several transport mechanisms in nanofluids, it is meaningful for the conservation equations to be in non-dimensional form. The advantages of non-dimensionalization are as follows: (i) non-dimensionalization gives freedom to analysis for any system irrespective of its material properties, (ii) one can easily understand the controlling flow parameters of the system, (iii) make a generalization of the size and shape of the geometry, and (iv) before doing an experiment one can get insight of the physical problem. These aims can be achieved through the appropriate choice of scales. As a scale of distance, we

choose the length of the cavity of the region under consideration measured along the x-axis. Thus, in order to reduce the dimensionless form of the governing equations (1)-(5) with boundary conditions (6)-(8), we incorporate the following dimensionless variables:

$$\left.\begin{array}{l} X = \dfrac{x}{L}, Y = \dfrac{y}{L}, U = \dfrac{uL}{\alpha_f}, V = \dfrac{vL}{\alpha_f}, \\[2mm] P = \dfrac{pL^2}{\rho_f \alpha_f^2}, \theta = \dfrac{T - T_c}{T_h - T_c}, \phi = \dfrac{C - C_0}{C_h - C_0} \end{array}\right\} \quad (9)$$

Introducing the relation (9) into equations (1)-(5), the governing dimensional equations can be written in the following dimensionless form:

$$\frac{\partial U}{\partial X} + \frac{\partial V}{\partial Y} = 0 \quad (10)$$

$$U \frac{\partial U}{\partial X} + V \frac{\partial U}{\partial Y} = -\frac{\partial P}{\partial X} + \Pr \nabla^2 U \\ + \Pr Ha^2 \left(V \sin\gamma \cos\gamma - U \sin^2\gamma \right) \quad (11)$$

$$U \frac{\partial V}{\partial X} + V \frac{\partial V}{\partial Y} = -\frac{\partial P}{\partial Y} \\ + \Pr \nabla^2 V + Ra \Pr (\theta - Nr\phi) \\ + \Pr Ha^2 \left(U \sin\gamma \cos\gamma - V \cos^2\gamma \right) \quad (12)$$

$$U \frac{\partial \theta}{\partial X} + V \frac{\partial \theta}{\partial Y} = \nabla^2\theta + Nb\left(\frac{\partial \phi}{\partial X} \frac{\partial \theta}{\partial X} \right) \\ Nb\left(+\frac{\partial \phi}{\partial Y} \frac{\partial \theta}{\partial Y} \right) + Nt\left[\left(\frac{\partial \theta}{\partial X}\right)^2 + \left(\frac{\partial \theta}{\partial Y}\right)^2 \right] \quad (13)$$

$$U \frac{\partial \phi}{\partial X} + V \frac{\partial \phi}{\partial Y} = \frac{1}{Le} \nabla^2\phi + \frac{Nt}{Le\, Nb} \nabla^2\theta \quad (14)$$

The dimensionless forms of the boundary conditions are as follows:
(i) On the round wall:

$$U = V = 0,\; \theta = 0,\; \phi = 1 \quad (15)$$

(ii) On the bottom wall:

Case-I: $U = V = 0, \theta = 1,\; \phi = 1 \quad (16a)$

Case-II: $U = V = 0, \theta = X(1-X), \phi = 1 \quad (16b)$

(iii) On the left vertical wall:

$$U = V = 0, \frac{\partial \theta}{\partial X} = 0,\; \phi = 1 \quad (17)$$

The parameters introduced in the above equations (11)-(14) are as follows:

$\Pr = \dfrac{\mu_f}{\rho_f \alpha_f}$ is the Prandtl number,

$Ha = B_0 L \sqrt{\dfrac{\sigma_f}{\mu_f}}$ is the Hartmann number,

$Ra = \dfrac{g\beta_f (1 - C_0)(T_h - T_c)L^3}{\alpha_f \upsilon_f}$ is the Rayleigh number,

$Nr = \dfrac{(\rho_p - \rho_f)(C_h - C_0)}{\rho_f \beta_f (T_h - T_c)(1 - C_0)}$ is the buoyancy ratio parameter,

$Nt = \dfrac{(\rho c_p)_p}{(\rho c_p)_f} \dfrac{D_T (T_h - T_c)}{T_c \alpha_f}$ is the thermophoresis parameter,

$Nb = \dfrac{(\rho c_p)_p}{(\rho c_p)_f} \dfrac{D_B (C_h - C_0)}{\alpha_f}$ is the Brownian

motion parameter and $Le = \dfrac{\alpha_f}{D_B}$ is the Lewis number.

Average Nusselt Number

The average Nusselt number for the bottom heated wall is calculated from the following expression:

$$Nu = -\int_0^1 \frac{\partial \theta}{\partial Y} dX \quad (18)$$

Thermophysical Properties of the Nanofluid

Kerosene-Cobalt nanofluid has been studied for the present work. The thermophysical properties of kerosene and cobalt are presented in Table 1.

Table 1. Thermophysical properties of kerosene and solid nanoparticle (cobalt).

Physical properties	kerosene	cobalt
c_p [J/kgK]	2090	420
ρ [kg/m^3]	780	8900
k [W/mK]	0.149	100
μ [Ns/m^2]	0.00164	-
β [1/K]	99×10^{-5}	1.3×10^{-5}
σ [W/mK]	6×10^{-10}	16.02×10^6
α [m^2/s]	9.14×10^{-8}	2.67×10^{-5}
Pr	23.004	-

Numerical Procedure

The finite element method is an efficient numerical and computational method for solving a variety of engineering and real world problems. The basic concept of the finite element method is to divide the domain or region of the problem into small connected patches, called finite elements. The collection of elements is called the finite element mesh. These finite elements are connected in a non overlapping manner, such that they completely cover the entire space of the problem. The advantages of finite element method are that it has ability to deal with complex 2D or 3D domains, and has higher accuracy and rapid convergence. Thus, the governing dimensionless equations (10)-(14) along with the boundary conditions (15)-(17) have been solved numerically by employing Galerkin weighted residual finite element method. The detail of this method is well described by Zienkiewicz and Taylor [12] and Uddin [13]. The six node triangular elements are used in this work for the development of the finite element equations. All six nodes are associated with velocities, temperature as well as isoconcentration; only the corner nodes are associated with pressure. This means that a lower order polynomial is chosen for pressure and is satisfied through the continuity equation. Then the nonlinear governing partial differential equations (i. e. conservation of mass, momentum and energy equations) are transferred into a system of integral equations by applying the Galerkin weighted residual method. The integration involved in each term of these equations is performed by using Gauss's quadrature method. The nonlinear algebraic equations so obtained are modified by imposition of boundary conditions. To solve the set of the global nonlinear algebraic equations in the form of a matrix, the Newton-Raphson iteration technique has been adapted through partial differential equation solver with MATLAB interface. The convergence criterion of the numerical solution along with error estimation has been set to $\left| \Phi^{m+1} - \Phi^m \right| \le 10^{-5}$, , where Φ is the general dependent variable (U, V, θ, ϕ) and m is the number of iteration.

Mesh generation

In the finite element method, the mesh generation is the technique to subdivide a domain into a set of sub-domains, called finite element, control volume, etc. The discrete locations are defined by the numerical grid, at which the variables are to be calculated. It is basically a discrete representation of the geometric domain on which the problem is to be solved. Meshing the complicated geometry makes the finite element method a powerful technique to solve the boundary value problems occurring in a range of engineering applications. Fig. 2 displays mesh configuration of the present physical domain with triangular finite elements.

Code validation

In order to check the accuracy of the numerical technique employed for the solution of the considered problem, the present numerical code was validated with the published study of Kent *et al.* [14].
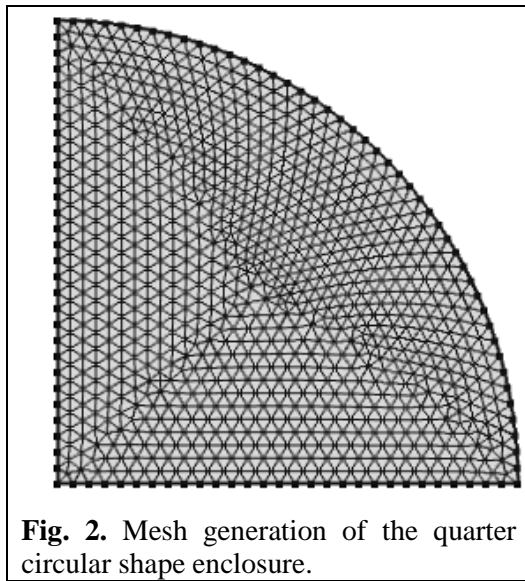
Fig. 2. Mesh generation of the quarter circular shape enclosure.

The physical problem studied by Kent *et al.* [14] was steady laminar natural convection inside a right triangular enclosure. The comparison of the results obtained by the present numerical code with those of Kent *et al.* [14] with respect to isotherms for different Rayleigh number is shown in Fig. 3. The computed results are in excellent agreement with the Kent *et al.* [14] solution. This validation boosts the confidence in the numerical outcome of the present study.

Numerical Results and Discussion

In this section, the obtained numerical results for natural convective heat transfer of cobalt-kerosene nanofluid in a quarter circular shape enclosure with uniform and non-uniform heated bottom wall cases are discussed. The parameters of the flow are calculated by their definition with the thermophysical properties of the nanoparticles and base fluid. The values of the Prandtl number is calculated for kerosene as 23.004. Let us consider $\Delta T = 10\text{K}$, $\Del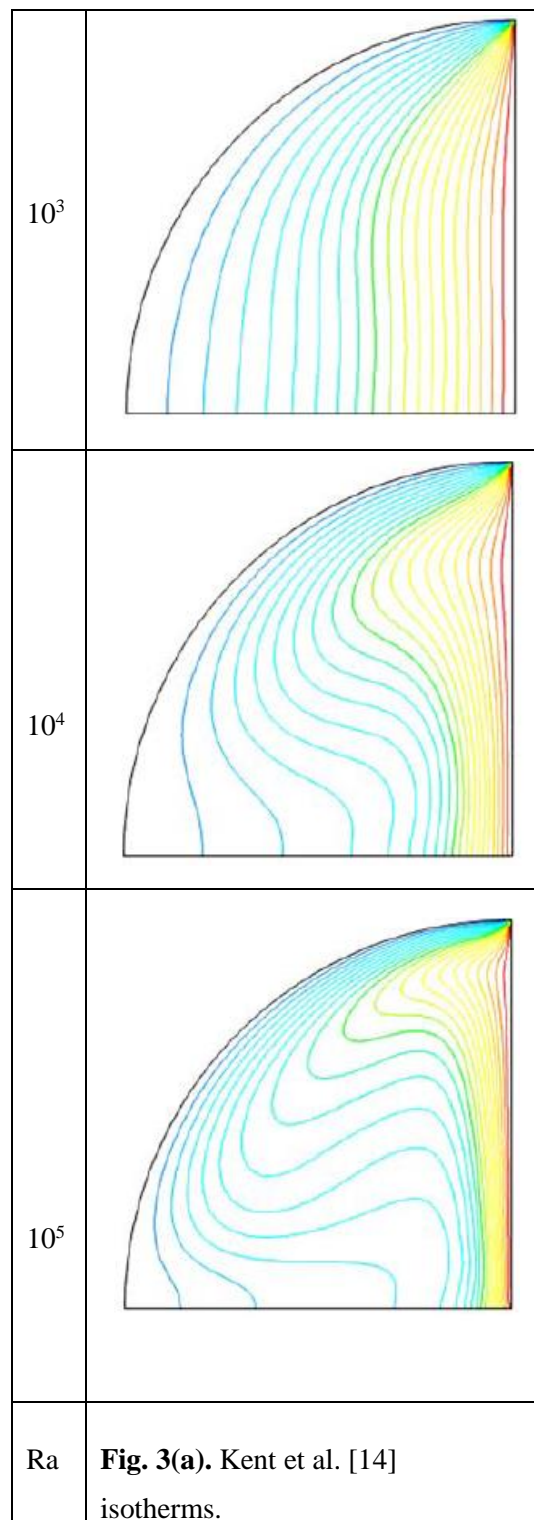ta C = 0.01$, $T_c = 300\text{K}$, $d_p = 50\text{nm}$. With these values, the physical parameters entered into the equations (11)-(14) for cobalt-kerosene nanofluid can be calculated as

follows: $Le = 17062$, $D_B = 5.3569 \times 10^{-12}$, $D_T = 8.9548 \times 10^{-12}$, $Nb = 1.3439 \times 10^{-6}$ and $Nt = 7.5387 \times 10^{-6}$. As the thermophysical properties of nanofluids depend on the thermophysical properties of nanoparticles and base fluids, the values of the above stated parameters will be different for each nanofluid. It is important to note that as the Brownian and thermophoretic diffusions strongly depend on the diameters of nanoparticles, the Brownian diffusion coefficient (D_B) and the thermal diffusion coefficient (D_T) changes with the size of the nanoparticles. The details concerning calculation of these parameter's values can be found in the works of Uddin et al. [7]. The other parameters such as the Rayleigh number (Ra), the Hartmann number (Ha) and magnetic field inclination angle (γ) are varied to analyze the flow and thermal characteristics of cobalt-kerosene nanofluid. Also, the values of the parameters especially Le, Nb and Nt will change according to the size of the particles, nanoparticles volume fraction and thermo physical properties of nanofluids. Streamlines, isotherms, and isoconcentrations as well as average Nusselt number are presented for a wide range of the controlling parameters for two different cases.
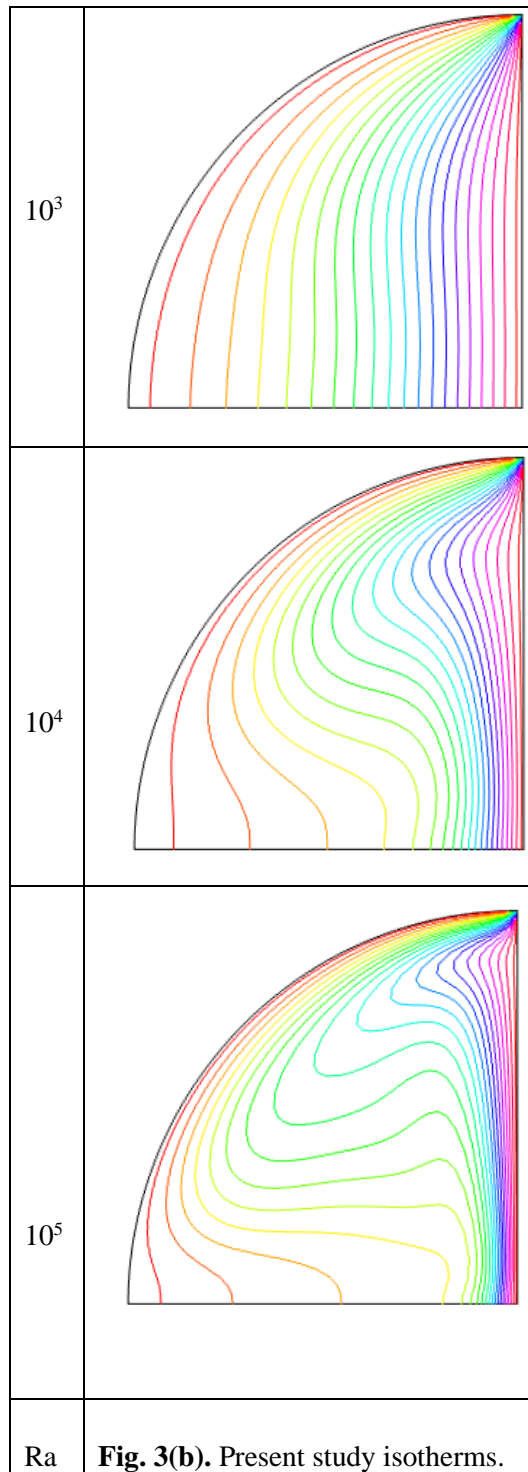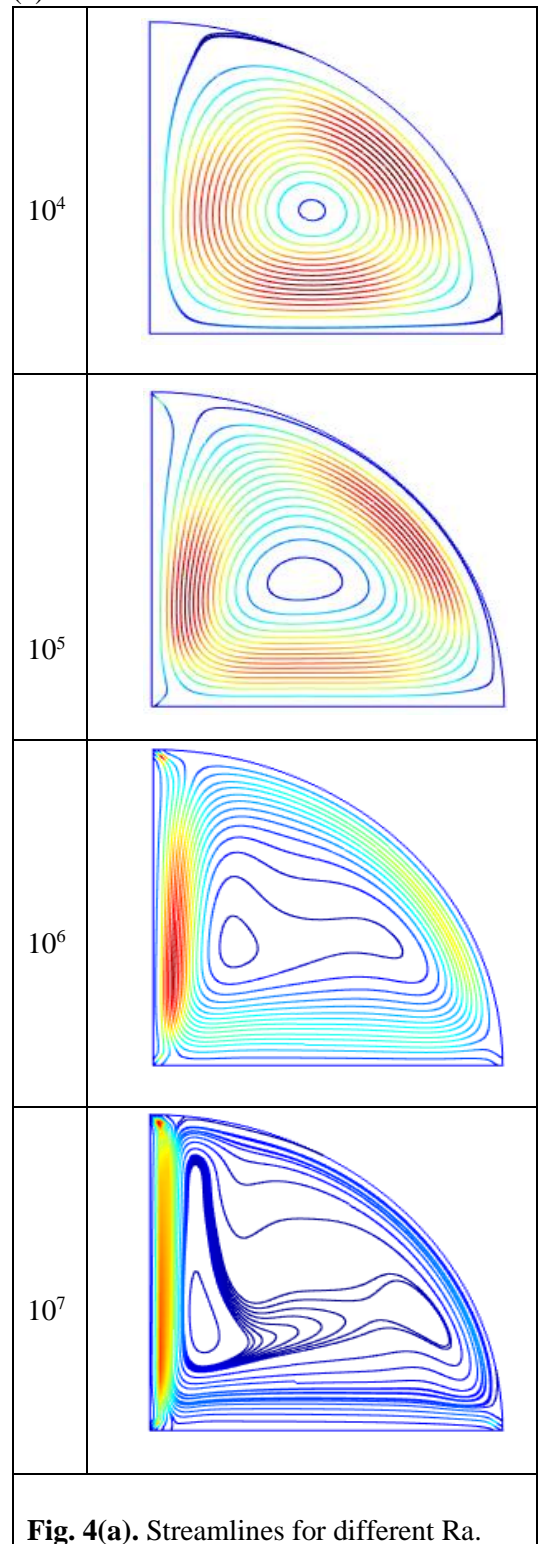
The effects of Rayleigh number Ra $(Ra = 10^4 - 10^7)$ on the streamlines have been displayed in Fig. 4(a)-(b) respectively when the bottom wall is heated uniformly as well as non-uniformly. The buoyancy-driven circulating flows within the enclosure are evident for all values of the Rayleigh number with two different cases. From this figure we see that the strength of these circulations increases as the Rayleigh number increases and this is due to the dominance of the natural convection. It is important to note that the vortex structure of the cell is circular at the center, but it turns to an elliptic as the Rayleigh number (Ra) increases to 10^7.

Another important change in the streamline pattern in case-II is that two counter-rotating circulation cells are present in the enclosure at $Ra = 10^4$. The convective streamline pattern is due to the different thermal boundary conditions which have been applied to the enclosure.
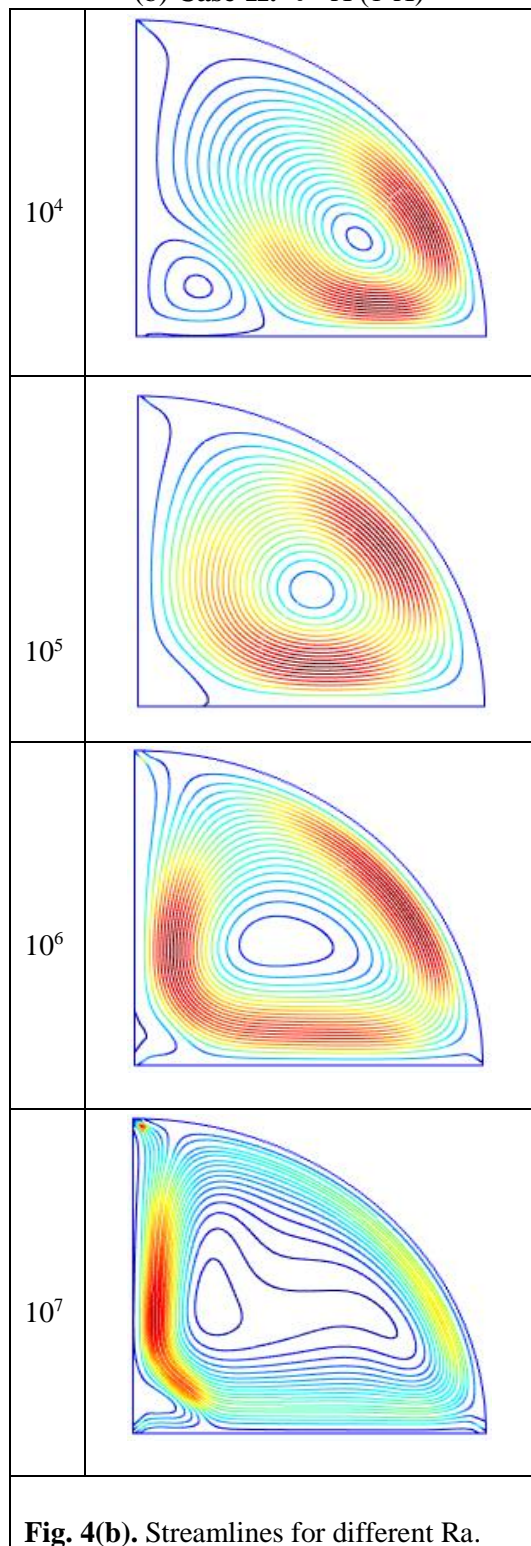
Fig. 5(a)-(b) display isotherm contours for Rayleigh number $Ra = 10^4 - 10^7$ with two different thermal boundary conditions at the bottom heated wall. From these figures, it is interesting to note that isotherms are more compressed near the right corner of the bottom wall. The close packing of isotherms tells us that at those regions, conduction is the primary mode of heat transfer. For higher values of Rayleigh number, the density of isotherms is less at the middle of the enclosure, which indicates relatively weaker convective heat transfer. As seen in Fig. 5(a) for case-I, the uniform heating of the bottom wall causes a finite discontinuity in Dirichlet type of the boundary conditions for the temperature distribution at the right edge of the bottom wall.
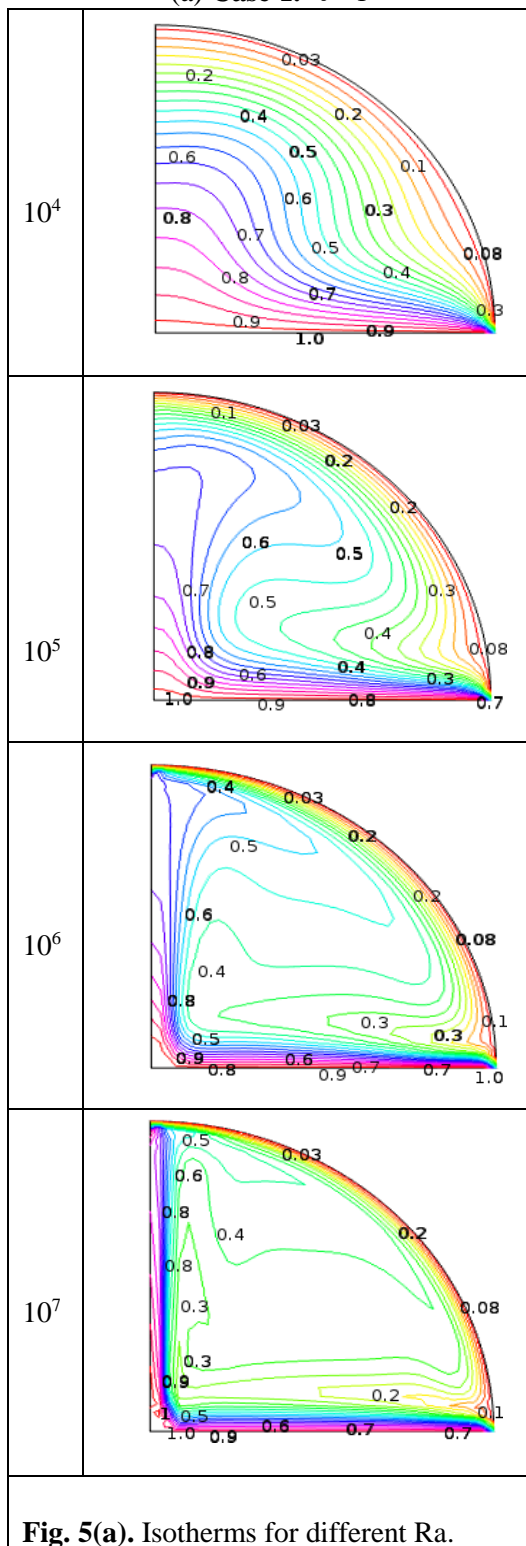

10^3	
10^4	
10^5	
Ra	**Fig. 3(a).** Kent et al. [14] isotherms.

(a) **Case-I:** $\theta = 1$

Ra	
10^3	
10^4	
10^5	

Fig. 3(b). Present study isotherms.

10^4	
10^5	
10^6	
10^7	

Fig. 4(a). Streamlines for different Ra.

(b) **Case-II:** $\theta = X(1-X)$	(a) **Case-I:** $\theta = 1$

Fig. 4(b). Streamlines for different Ra.

Fig. 5(a). Isotherms for different Ra.

54

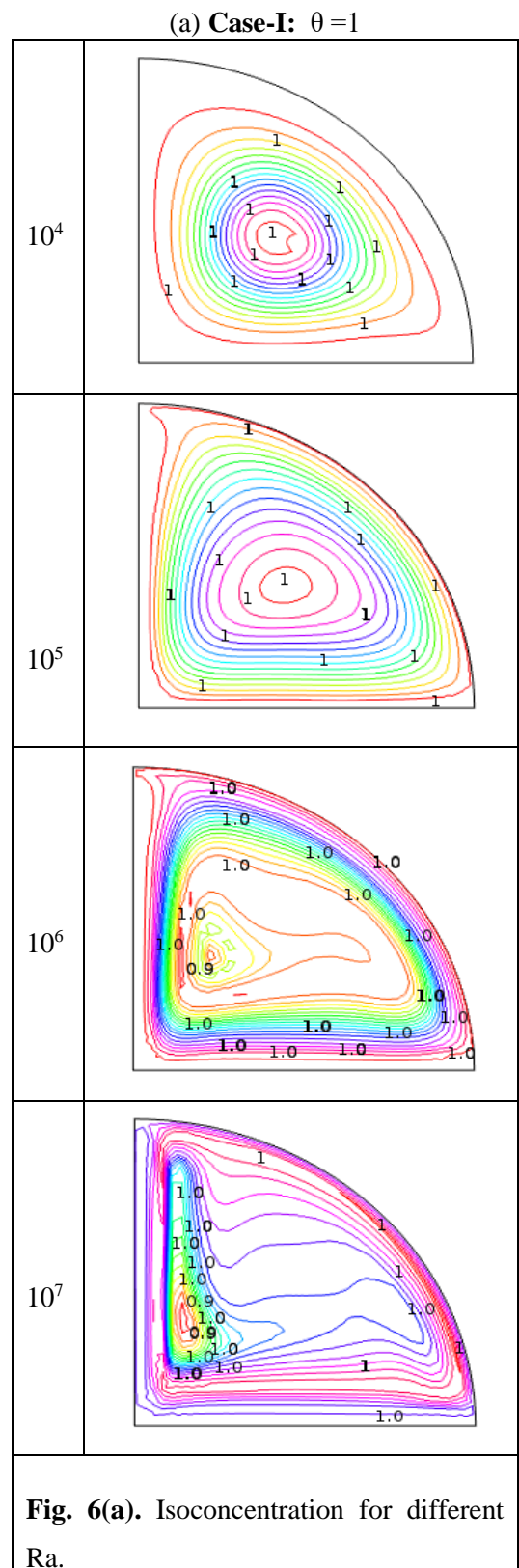(b) **Case-II:** θ =X (1-X)   (a) **Case-I:** θ =1
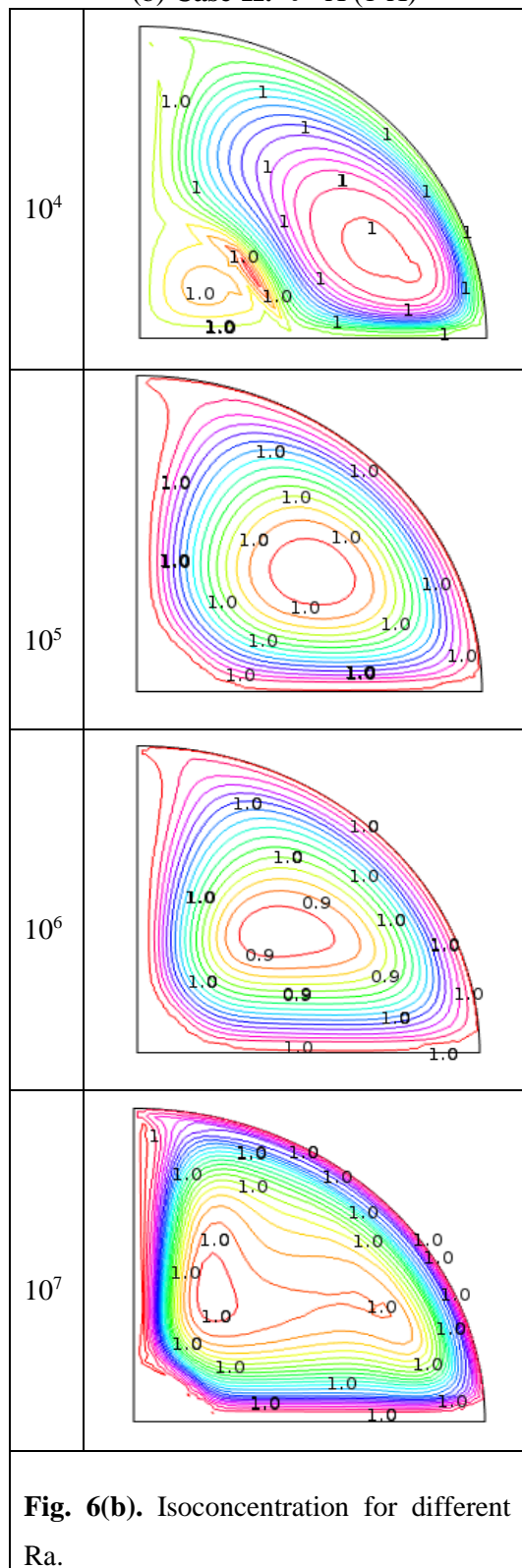

Fig. 5(b). Isotherms for different Ra.

Fig. 6(a). Isoconcentration for different Ra.

55

(b) **Case-II:** θ =X (1-X)   (a) **Case-I:** θ =1

10^4	
10^5	
10^6	
10^7	

0^0	
60^0	
90^0	
180^0	

Fig. 6(b). Isoconcentration for different Ra.

Fig. 7(a). Streamlines for different γ.

(b) **Case-II:** $\theta = X(1-X)$ (a) **Case-I:** $\theta = 1$

0^0		0^0	
60^0		60^0	
90^0		90^0	
180^0		180^0	
Fig. 7(b). Streamlines for different γ.		**Fig. 8(a).** Isotherms for different γ.	

Fig. 7(b). Streamlines for different γ.
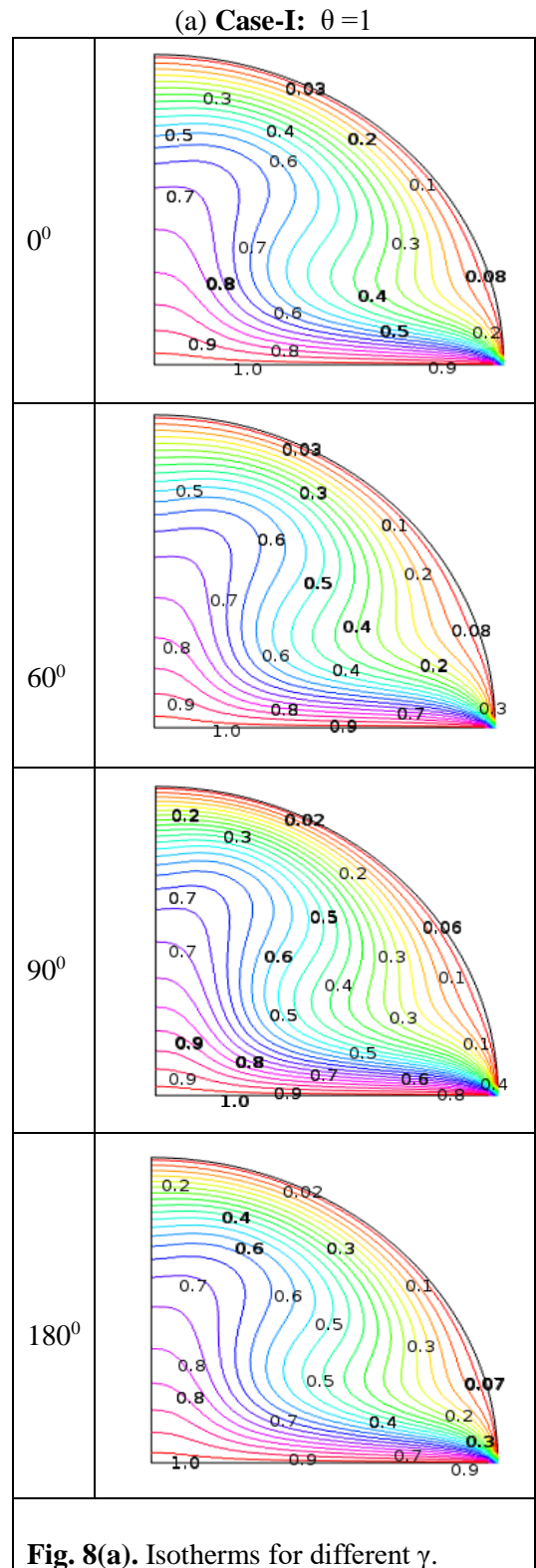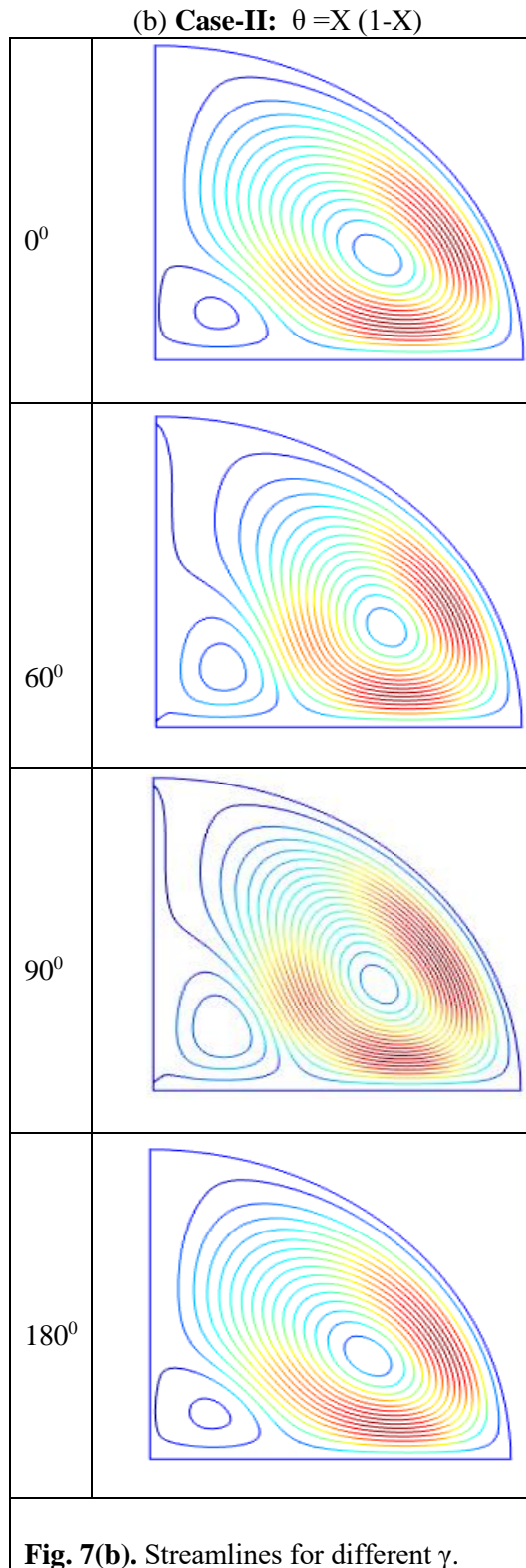
Fig. 8(a). Isotherms for different γ.

(b) **Case-II:** $\theta = X(1-X)$ (a) **Case-I:** $\theta = 1$

0^0		0^0	
60^0		60^0	
90^0		90^0	
180^0		180^0	
Fig. 8(b). Isotherms for different γ.		**Fig. 9(a).** Isoconcentration for different γ.	

58
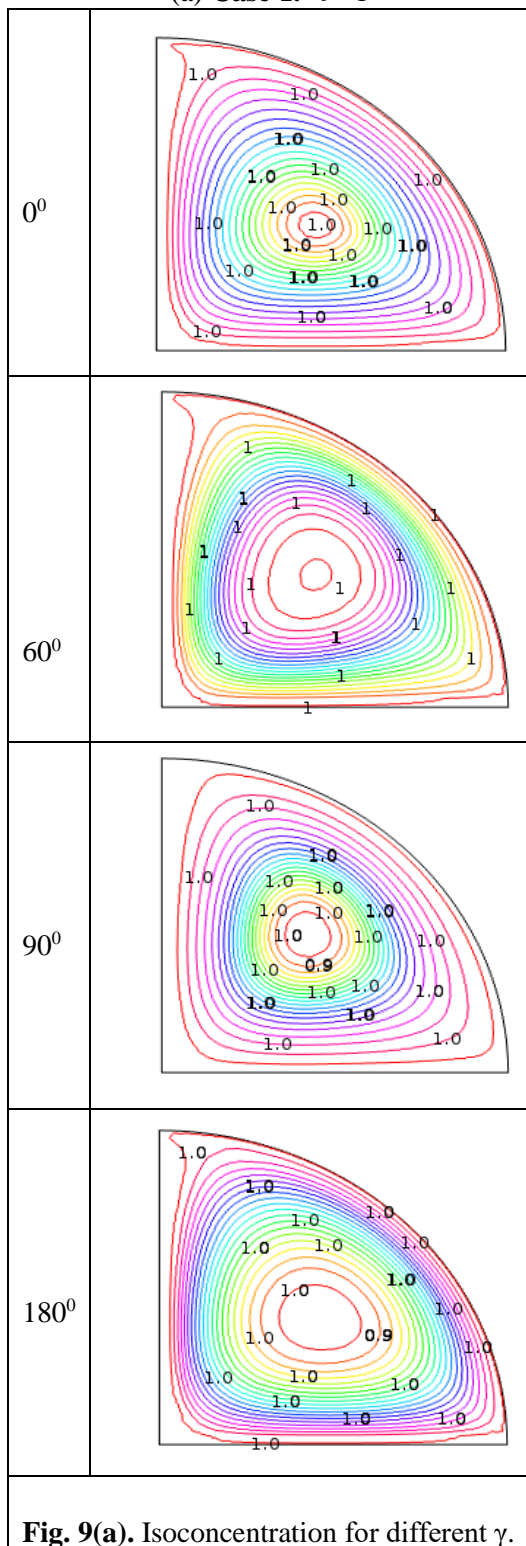
(b) **Case-II:** $\theta = X(1-X)$

(a) **Case-I:** $\theta = 1$

0^0	
60^0	
90^0	
180^0	
Fig. 9(b). Isoconcentration for different γ.	

0	
30	
60	
100	
Fig. 10(a). Streamlines for different Ha.	

59

	(b) **Case-II:** $\theta = X(1-X)$		(a) **Case-I:** $\theta = 1$
0		0	
30		30	
60		60	
100		100	
Fig. 10(b). Streamlines for different Ha.		**Fig. 11(a).** Isotherms for different Ha.	

(b) **Case-II:** θ =X (1-X)   (a) **Case-I:** θ =1

Fig. 11(b). Isotherms for different Ha.

Fig. 12(a). Isoconcentration for different Ha.

61

(b) **Case-II:** θ =X (1-X)

0	
30	
60	
100	

Fig. 12(b). Isoconcentration for different Ha.

Fig. 13. Average Nusselt number for Ra.
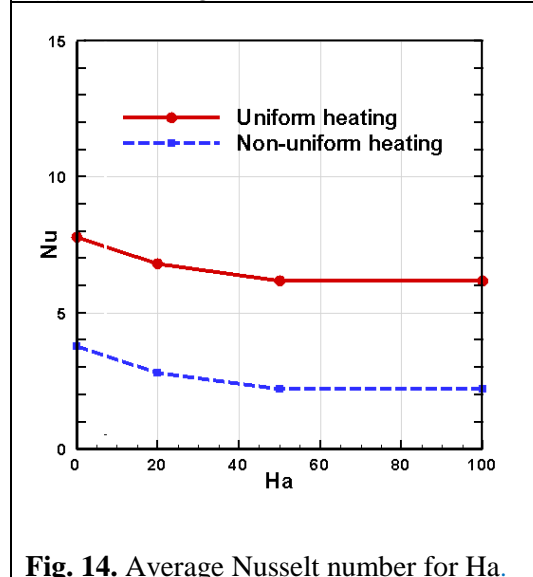
Fig. 14. Average Nusselt number for Ha.

In contrast, the non-uniform heating removes the singularity at the right edge of the bottom wall as observed in Fig. 5(b) for case-II. For relatively higher values of Rayleigh number, the isotherms are quite dispersed throughout the enclosure. According to Fig. 5(a) for case-I, isotherms are uniformly distributed which shows that the conduction heat transfer is dominant. By increasing the Rayleigh number *Ra*, the isotherms become

more distorted due to the stronger convection effects. An increase in the Rayleigh number intensifies the convection regime which leads to the enhancement of the heat transfer rate.

The effects of the Rayleigh number Ra on the isoconcentrations or concentration distribution of nanoparticles in the quarter circular enclosure have been displayed in Fig. 6(a)-(b) for two different thermal boundary conditions on the bottom heated wall. As seen, the concentration of nanoparticles in the vicinity of the bottom heated wall is low, and in contrast, it is high in the vicinity of the round cold wall for higher values of Rayleigh number. This distribution of concentration of nanoparticles is due to the thermophoresis forces, which tend to move the nanoparticles from the hot wall toward the cold one. In addition, Fig. 6(a)-(b) clearly show that the concentration gradient of nanoparticles near the walls is high, but the concentration of nanoparticles in the core region of the enclosure is almost uniform. Therefore, 50 nm size nanoparticles are uniform and stable in the solutions. The high concentration gradients next to the hot and cold walls are due to the high values of Rayleigh number. It is also interesting to note that the pattern of isoconcentrations in a quarter circular enclosure is almost similar to that of streamlines. This kind of outcome is very rare in other types of enclosure. This clearly indicates that the quarter circular shape enclosure plays a very important role to obtain full-bodied flow and uniform concentration of nanoparticles.

The influence of magnetic field inclination angle (γ) on streamlines, isotherms and isoconcentrations is displayed in Fig. 7-9 respectively for both uniformly and non-uniformly heated bottom wall cases. The magnetic field inclination angle has been varied from 0^0 to 180^0. At a first glance, it can be observed that the magnetic field controls the flow pattern of the nanofluid. From Fig. 7(a)-(b), we observe that the patterns of streamlines do not change

significantly but the strength of the vortices increases. Streamlines spread in the entire enclosure with the increase of the magnetic field inclination angle. The flow direction changes with the magnetic field inclination angle. But for case-II, two opposite rotational vortices change their position according to the direction of magnetic field which clearly shows that using magnetic field, the flow direction as well as heat transfer can be controlled. Again from Fig. 8(a)-(b), we see that, unlike the flow field, the temperature field is not affected much by the orientation of the magnetic field. The isotherms are almost equally spaced between the hot and cold walls. The thermal boundary layer becomes slightly thick and the isotherms are more concentrated for the uniformly heated wall than the non-uniformly heated wall. From Fig. 9 (a)-(b), it is clearly seen that the magnetic field inclination angle significantly affects the loops of the isoconcentration curves. The loops of the isoconcentration curves elongates according to the direction of the magnetic field. This happens because motion or traces of nanoparticle are controlled by the magnetic intensity.

The influence of the Hartmann number Ha $(Ha = 0 - 100)$ on the streamlines, isotherms and isoconcentrations is shown in Fig. 10-12, respectively, for both uniformly and non-uniformly heated bottom wall cases. As the value of the Hartmann number is increased (stronger magnetic field is applied), strength of the flow inside the cavity decreases. This outcome is supported by many previous researches. Physical reasoning behind this result is that, an externally applied magnetic field imposes a strong field over moving fluid that has magnetic susceptibility. It results in generating a Lorentz force field which has a nature to oppose the movement of fluid. This force field weakens the streamlines inside the cavity as observed in Fig. 10(a)-(b). From Fig. 11(a)-(b), the effect of the Hartmann number (Ha) is more prominent which gives indication of the

mode of heat transfer. As it can be observed that for $Ha = 0$ and $Ha = 30$, the isotherms pattern are more compressed near the bottom heated wall which is an indication of strong convection. But when the values of Ha are increased $(Ha = 60 \text{ or } Ha = 100)$, isotherms are almost parallel which means that a raising Hartmann number is acting against convection inside the cavity. From Fig. 12 (a)-(b), we see that the isoconcentration curves are almost uniformly distributed in the entire enclosure for $Ha = 0 - 30$, but for higher values of Ha, isoconcentration curves are clustered near the cold round wall of the enclosure. This is due to thermophoresis effect of the nanoparticles inside the enclosure.

Average Nusselt number for different values of Rayleigh number (Ra) and Hartmann number (Ha) for both uniform and non-uniform heating bottom wall are shown in Fig. 13, and Fig. 14, respectively. General observation is that the average Nusselt number increases with the increasing values of Rayleigh number, it decreases with the increasing values of the Hartmann number, and it is utilized to represent the overall heat transfer rate within the domain. But the highest heat transfer rate is observed for the uniformly bottom heated wall case.

Conclusions

In this paper, the problem of steady laminar natural convective flow and heat transfer of cobalt-kerosene nanofluid inside a quarter circular enclosure under the influence of an oriented magnetic field is studied using a two-component non-homogeneous mathematical model. The governing nonlinear partial differential equations are transformed into the dimensionless form using suitable non-dimensional quantities. The Galerkin weighted residual based finite element method has been used to solve the governing dimensionless equations. The numerical results of the flow, thermal and concentration behaviors are displayed graphically in terms of the streamlines, isotherms and isoconcentrations All numerical results are discussed from the physical point of view. From the numerical simulations, the major outcomes are listed below:

1. Variation of average Nusselt number is directly proportional to the variation of Rayleigh number *(Ra)* for both uniformly and non-uniformly heated bottom wall cases.
2. Variation of average Nusselt number is inversely proportional to the variation of Hartmann number *(Ha)* for both uniformly and non-uniformly heated bottom wall cases.
3. The uniform heating of the bottom wall of the enclosure exhibits a higher heat transfer rate.
4. A quarter circular shape enclosure plays a very important role to obtain a full-bodied flow and uniform concentration of nanoparticles.

Nomenclature

B_0	magnetic field strength
c_p	specific heat at constant pressure
C	nanoparticle volume fraction
D_B	Brownian diffusion coefficient
D_T	thermophoretic diffusion coefficient
g	gravitational acceleration
Ha	Hartmann number
k	thermal conductivity
L	length of the cavity
Le	Lewis number
Nb	Brownian motion parameter
Nr	buoyancy ratio parameter
Nt	thermophoresis parameter
Nu	Average Nusselt number
p	dimensional pressure
P	dimensionless pressure
Pr	Prandtl number
Ra	Rayleigh number
T	temperature
u,v	dimensional velocity components
U,V	dimensionless velocity components
x,y	dimensional coordinates
X,Y	dimensionless coordinates
α	thermal diffusivity
β	coefficient of thermal expansion
γ	magnetic inclination angle
σ	electric conductivity
θ	dimensionless temperature
ϕ	normalized nanoparticle volume fraction
μ	dynamic viscosity
ρ	density
$\left(\rho c_p\right)$	heat capacity
Subscripts	
c	condition at cold wall
f	base fluid
h	condition at heated wall
p	solid nanoparticle

References

[1] Subbarayalu G, Velappan S. Magneto convection in tilted square cavity with differentially thermally active vertical walls. J Math Statist 2011; 7(2):149-56.

[2] Pirmohammadi M, Ghassemi M. Effect of magnetic field on convection heat transfer inside a tilted square enclosure. Int Commun Heat Mass Transfer 2009;36:776-80.

[3] Lo DC. High-resolution simulations of magnetohydrodynamic free convection in an enclosure with a transverse magnetic field using a velocity–vorticity formulation. Int Commun Heat Mass Transfer 2010;37:514-23.

[4] Bakhshan Y, Ashoori H. Analysis of a fluid behavior in a rectangular enclosure under the effect of magnetic field. Int J Mech Aerosp Eng 2012;6:161-65.

[5] Kakaç S, Pramuanjaroenkij A. Review of convective heat transfer enhancement with nanofluids. Int J Heat Mass Transfer 2009;52:3187-96.

[6] Sarit K, Choi U, Wenhua Y, Pradeep T. Nanofluids, science and technology. John Wiley & Sons; 2008.

[7] Uddin MJ, Al Kalbani KS, Rahman M M, Alam MS, Al-Salt, Eltayeb IA, Fundamentals of nanofluids: evolution, applications and new theory. J Biomath Sys. Biol 2016;2(1):1-32.

[8] Choi SUS. Enhancing thermal conductivity of fluids with nanoparticles. In: Siginer DA, Wang HP, editors. ASME FED; 1995. p. 99-105.

[9] Buongiorno J. Convective transport in nanofluids. ASME J Heat Trans 2006; 128:240-50.

[10] Sheremet MA, Pop I. Free convection in a triangular cavity filled with a porous medium saturated by a nanofluid; Buongiorno's mathematical model. Int J Numer Method H 2015;25:1138-61.

[11] Rahman MM, Alam MS, Al-Salti N, Eltayeb IA. Hydromagnetic natural convective heat transfer flow in an isosceles triangular cavity filled with nanofluid using two-component nonhomogeneous model. Int J Therm Sci 2016;107:272-88.

[12] Zienkiewicz OC, Taylor RL. The finite element method. 4th ed., McGraw-Hill; 1991.

[13] Uddin MB. Magnetic field effect on double-diffusive mixed convection in a lid driven trapezoidal enclosure for unsteady flow [M. Thesis]. Dhaka: BUET; 2015.

[14] Kent EF, Asmaz E, Ozerbay S. Laminar natural convection in right triangular enclosures. Heat Mass Transfer 2007;44:187-200.